PHILOSOPHICAL TRANSACTIONS OF THE ROYAL SOCIETY A

rsta.royalsocietypublishing.org

Advancing predictive models for particulate formation in turbulent flames via massively parallel direct numerical simulations

Fabrizio Bisetti[1], Antonio Attili[1] and Heinz Pitsch[2]

[1]Clean Combustion Research Center, King Abdullah University of Science and Technology, Thuwal 23955, Kingdom of Saudi Arabia
[2]Institute for Combustion Technology, RWTH Aachen University, Aachen 52056, Germany

Research

Cite this article: Bisetti F, Attili A, Pitsch H. 2014 Advancing predictive models for particulate formation in turbulent flames via massively parallel direct numerical simulations. *Phil. Trans. R. Soc. A* **372**: 20130324. http://dx.doi.org/10.1098/rsta.2013.0324

One contribution of 13 to a Theme Issue 'Aerodynamics, computers and the environment'.

Subject Areas:
energy, mechanical engineering, power and energy systems

Keywords:
turbulent combustion, soot, direct numerical simulation, intermittency

Author for correspondence:
Fabrizio Bisetti
e-mail: fabrizio.bisetti@kaust.edu.sa

Combustion of fossil fuels is likely to continue for the near future due to the growing trends in energy consumption worldwide. The increase in efficiency and the reduction of pollutant emissions from combustion devices are pivotal to achieving meaningful levels of carbon abatement as part of the ongoing climate change efforts. Computational fluid dynamics featuring adequate combustion models will play an increasingly important role in the design of more efficient and cleaner industrial burners, internal combustion engines, and combustors for stationary power generation and aircraft propulsion. Today, turbulent combustion modelling is hindered severely by the lack of data that are accurate and sufficiently complete to assess and remedy model deficiencies effectively. In particular, the formation of pollutants is a complex, nonlinear and multi-scale process characterized by the interaction of molecular and turbulent mixing with a multitude of chemical reactions with disparate time scales. The use of direct numerical simulation (DNS) featuring a state of the art description of the underlying chemistry and physical processes has contributed greatly to combustion model development in recent years. In this paper, the analysis of the intricate evolution of soot formation in turbulent flames demonstrates how DNS databases are used to illuminate relevant physico-chemical mechanisms and to identify modelling needs.

Royal Society Publishing

1. Introduction

In 2011, combustion of coal, oil and natural gas provided 81% of world energy. Even in the event of a drastic change in the energy landscape, the share of energy consumption from fossil fuels is projected not to fall below 65% until 2035 [1]. Energy demand is moving to the emerging economies, which are now the major drivers for the current increase in global energy use. In China, India and the Middle East, the growth in energy demand is met by the fast-paced installation of new fossil fuel power plants. Harmful emissions from combustion devices include carbon dioxide, unburned hydrocarbons, carbon monoxide, nitrogen oxides and particulates. As is well recognized, anthropogenic carbon dioxide is a greenhouse gas and a major contributor to global warming, so that the abatement of its emissions from combustion devices is of great importance within the wider climate change goals.

Throughout the last century, combustion technology has evolved in response to the need to reduce the emission of pollutants and increase efficiency [2]. Recently, and largely due to tightening regulations, the goal of curtailing emissions of carbon and other hazardous pollutants has gained more urgency and a diverse portfolio of combustion strategies is under consideration, including improvements in efficiency, flexibility towards alternative fuels such as biofuels and hydrogen and suitability of the combustion process to economical carbon capture approaches.

Combustion is a mature technology and further improvements are difficult to realize. In particular, improvements in efficiency through the adoption of novel combustion regimes, such as ultra-lean combustion, and the implementation of a robust oxi-fuel combustion process in stationary combustors, which would enable economical carbon capture, are challenging. In most technical devices, combustion occurs in the turbulent flow regime, which is characterized by unsteady, three-dimensional and intermittent flow fields [3]. The conversion of fuel and oxidizer into heat and product species proceeds through a complex network of reactions, which are often confined to thin, front-like regions of the flow due to the exponential dependence of reaction rates on temperature and the fast conversion of fuel and oxidizer to products compared with mixing. It is well established [4] that turbulence affects the transport of heat and mass near and within such thin reaction fronts, impacting the rates of chemical reaction and controlling processes of great practical relevance such as pollutant formation, flame ignition and extinction, flame stabilization, burning rate and combustion instabilities [2]. Owing to severe experimental limitations and the need to contain development time and cost, the design of combustion devices leverages computational fluid dynamics (CFD), presently in the form of Reynolds-averaged Navier–Stokes (RANS) calculations.

In the past decades, there have been important efforts in the development of combustion models for large eddy simulation (LES) [5] and, largely as a result of significant advancements brought by the turbulent combustion scientific community, LES is emerging as a convincing alternative to RANS in the design-cycle of modern combustion devices [6]. On account of its ability to resolve the unsteady motion of the large scales of the flow, LES has the potential to improve the prediction of pollutant emissions and unsteady combustion events, such as ignition, extinction and instabilities [5], and is capable of accurate predictions of flame dynamics and mixing patterns in configurations of industrial relevance [6]. Thus, the development and appraisal of subfilter closure models for LES of turbulent combustion is an important and active field of research [5], which holds the yet unrealized potential for supporting the broad climate change goals of carbon dioxide and particulate abatement.

The formation of pollutants is governed by strong nonlinearities and wide ranges of time scales with substantial sensitivities towards the local flow environment and mixing rates. Despite the ever more pressing need to optimize the combustion process and control pollutant formation in technical devices, the combustors' efficiency and emission yields cannot be predicted reliably by available CFD approaches. In order to develop accurate LES models for pollutant formation, existing subfilter closure approaches must be assessed and novel strategies devised. These modelling activities require a remarkably detailed insight into the close coupling

between turbulent mixing and the chemical processes leading to the formation of pollutants. For the most part, the completeness of the data necessary for LES model development is beyond the reach of experimental diagnostics, so that computational science and, in particular, large scale direct numerical simulations (DNS) are critical components of any successful CFD effort in turbulent combustion [5]. It is envisaged that an integrated approach combining experiments and DNS of pollutant formation in turbulent flames will sustain LES subfilter model development, thereby contributing in practical ways to the design of more efficient and cleaner combustion devices.

The availability of high performance computing systems capable of tera- and peta-flop scale calculations has enabled an important number of DNS studies of turbulent combustion at moderate Reynolds number [7]. The data provide a detailed, complete and fully resolved (in time and space) description of combustion in turbulent flows. DNS enables probing the fields of velocity, temperature and species concentrations concurrently and instantaneously. Thus, DNS studies have played a well-recognized pivotal role in the advancement of our understanding of turbulent combustion in the last 10 years or so [2].

The most recent DNS databases of turbulent flames excel in quality and scope and have facilitated the formulation of novel subfilter closures. In addition, those databases have supported the assessment of selected assumptions and components of existing subfilter models with tangible improvements to the predictions. Pertinent examples include the recent advances in methods and models for the subfilter probability density function [8], transported filtered density function [9], scalar dissipation rate [10] and premixed flame propagation [11–13]. In the context of subfilter model development, spatially and temporally resolved joint statistics of multiple fields and their gradients are desirable, so that the data available from DNS are unique and unmatched even by the most advanced laser-based diagnostics for turbulent combustion [14].

Among various other pollutants, such as nitrogen oxides and unburnt hydrocarbons, anthropogenic carbon-based particulate ('soot') is highly detrimental to human health [15] and the environment [16], and stringent regulations on its emissions from combustion devices are in place in most countries worldwide. Soot is an aerosol consisting of tiny carbonaceous particles clustered in aggregates up to about 1 μm in size [17]. The diameter of the 'primary' particles ranges from 10 to 30 nm and there are a few hundred monodisperse primaries in a large soot aggregate. Soot primary particles originate from large polycyclic aromatic hydrocarbon (PAH) species [18], such as naphthalene, pyrene and coronene. PAHs develop in the gas phase from a hierarchy of smaller molecules formed during the decomposition of hydrocarbon fuels under fuel-rich conditions. Upon formation, soot primaries grow further by addition of PAH molecules and by chemical reactions on the particles' surface. Collisions among particles lead to a rapid decrease in the soot number density and the formation of aggregates. Depending on the flow configuration, soot aggregates may lose mass due to the attack of molecular oxygen and hydroxyl radical onto the carbon. As indicated by experimental [19,20] and computational [21–24] studies, the formation and growth of soot in flames is affected strongly by turbulence, leading to 'soot–turbulence–chemistry interaction'.

LES studies of turbulent sooting flames are few [25–27], reflecting the limited understanding of the underlying physics of soot formation in turbulent flames and general lack of data. Concurrent, instantaneous, pointwise measurements of soot quantities, such as soot number density and volume fraction, together with the temperature and concentration of gas-phase species are needed to support subfilter model development. For the most part, these quantities are not accessible experimentally and their quantitative characterization in turbulent sooting flames is well beyond the capabilities of current diagnostics [20]. Gas-phase species of interest include large soot precursor species, which are not amenable to laser-based measurement techniques in use in turbulent combustion studies. Moreover, the presence of soot prevents the usage of many advanced diagnostics for temperature and mixture fraction, which have been instrumental in the characterization of soot-free turbulent flames in the past [14]. It is clear that the role of DNS in the development of LES closures for soot formation in turbulent flames is invaluable and fills a large knowledge gap left by incomplete experimental databases.

There exists a growing number of DNS studies of soot formation in turbulent flames [21–24,28]. Bisetti *et al.* [21] performed a DNS of soot formation and growth in a two-dimensional turbulent non-premixed flame subject to decaying turbulence. Their work [21] improved upon previous studies by considering a detailed soot model based on elementary physical processes and rates [29], rather than a semi-empirical approach. For the first time in a DNS of turbulent combustion, Bisetti *et al.* [21] included finite-rate chemistry describing the formation of PAH species and pointed to the mechanisms of soot–turbulence–chemistry interaction in turbulent flames. Their findings were instrumental in guiding a recently proposed LES closure approach [26,30].

The work by Bisetti *et al.* [21] has been recently extended to a campaign of DNSs of soot formation in realistic, three-dimensional, temporally evolving turbulent non-premixed planar jet flames [22,23]. Small-scale turbulence differs in two and three dimensions [3] and is central to soot–turbulence–chemistry interaction. These recent DNS studies [22,23] constitute the state of the art in DNS of turbulent combustion in terms of scope, physical models and numerical methods for massively parallel reactive flow simulations. The calculations [22,23] feature 500 million grid points and consumed more than 50 million cpu-hours on 65 536 cores of an IBM Blue Gene/P system, generating in excess of 100 TB of data. The resulting DNS database underlies the analysis presented here.

This paper addresses the formation of soot in turbulent non-premixed flames, demonstrating the usefulness of DNS databases in the development of LES-based combustion models for complex processes such as the formation of pollutants. Results from large-scale DNS studies are used to shed light on physico-chemical processes, identify modelling challenges and provide guidelines for model development.

2. Flow configuration, models and methods

Three-dimensional, temporally evolving turbulent non-premixed planar jet flames are considered [22,23]. The fuel jet is *n*-heptane diluted in 85% nitrogen at 400 K and is surrounded by air at 800 K, yielding a stoichiometric mixture fraction $Z_{st} = 0.147$. The pressure is atmospheric.

The gas-phase hydrodynamics are modelled with the reactive Navier–Stokes (N–S) equations in the low Mach number limit [31]. The transport of heat and mass is described using the Hirschfelder and Curtiss approximation to the diffusive fluxes and all properties are computed with a mixture-average approach [32]. Combustion is modelled using a mechanism for the oxidation of *n*-heptane comprising 47 species and 290 reactions [21]. The mechanism includes the intermediate species and pathways leading to the formation of naphthalene, the smallest PAH soot precursor consisting of two benzene rings.

Soot particles and aggregates are characterized by their volume (V) and surface area (S) [33], and a moment method is used as a statistical approach to describe the soot particle number density function in terms of these parameters. A common closure approximation for the unknown moments appearing in the formulation is the high-order inter- or extrapolation in moment space (method of moments with interpolative closure, MOMIC) [34]. Here, the so-called hybrid method of moments [35] is used, which combines MOMIC with a quadrature approach and is particularly well suited for multi-modal particle distributions in a multivariate description [33,36].

The equations for the soot moments include the unsteady, convective and source terms only, as soot transport is characterized by a very high Schmidt number and diffusive mass fluxes are neglected [21]. The contribution of thermophoresis is also unimportant in comparison to that of convection [21] and is not included. The source term describes aerosol processes [29,37,38]: nucleation, coagulation, growth (condensation and surface reactions) and oxidation of soot particles. More details on the physical and chemical processes and model equations for the evolution of soot and its precursors are available in [21,22].

The gas velocity and reactive scalar fields are solved with state of the art algorithms for variable density, low Mach number reactive flows. For more details, see [22,39]. The system of

equations for the soot moments is solved with a Lagrangian particle method, which represents the soot fields with an ensemble of notional particles [40]. The Lagrangian method prevents the moment realizability problem related to errors in the advective fluxes [41] and circumvents the weak stability and poor accuracy of conventional Eulerian methods due to the stiffness of the source terms in the soot evolution equations [42]. While important in large-scale industrial burners, the contribution of radiative heat transfer from soot and the gas phase is negligible in the present configuration due to the small physical size of the domain and is not included in the energy equation.

Three flow configurations are simulated with varying hydrodynamic time scale, defined as the ratio of the initial jet width to the mean centreline velocity. The physical sizes of the domain and the velocities are rescaled among the three cases, while keeping the Reynolds number of the flow constant. All three configurations feature the same composition and temperature of the streams. The resulting three flow fields are hydrodynamically similar and are characterized by three Damköhler numbers: $Da_{\mathrm{H}} = 2\,Da_{\mathrm{M}} = 4\,Da_{\mathrm{L}}$, where Da_{H} indicates the configuration with the slowest hydrodynamic time scale. Note that each chemical reaction and soot process has its own rate and associated Da number. As the chemistry and soot processes are unchanged among the three cases, all Da numbers vary equally upon rescaling the hydrodynamic time scale. For more details, the reader is referred to [23].

The configuration consists of a planar jet, modelled as a temporally evolving flow. The flow is periodic in the streamwise (x) and spanwise (z) directions and open boundary conditions are prescribed in the crosswise direction (y). A realization of a fully developed turbulent channel flow at $Re_\tau = 390$ is used to initialize the velocity field in the fuel core. The jet Reynolds number is $(U_{\mathrm{c}} - U_{\mathrm{co}})H/\nu \approx 15\,000$, where H is the initial jet width and U_{c} and U_{co} are the centreline and coflow velocity, respectively. The domain spans $L_x = 9.4$, $L_y = 10.5$ and $L_z = 4.7$ cm and is discretized with $1024 \times 1024 \times 512 \approx 500$ million points. The mesh is homogeneous in all directions, yielding a mesh spacing $h = 91\,\mu$m for $|y/H| \leq 2.8$. Outside of this region, the mesh is stretched slightly in the crosswise direction. The mesh size h results in a spatial resolution below the minimum average Kolmogorov scale ($\eta = 110\,\mu$m and $h/\eta \approx 0.82$) and the thin reaction fronts are adequately resolved. Approximately 1 billion notional particles describe soot quantities in the Lagrangian method. For more details, see [22].

The simulation of soot formation presents unique numerical challenges in the context of DNS of turbulent combustion given the long physical times required for the formation and growth of soot. For example, the power stroke of a passenger-car Diesel engine at 1750 r.p.m. lasts approximately 17 ms and similar time scales are associated with the evolution of soot in aeroderivative combustors, while the time scales that need to be resolved for accuracy are of the order of $\mathcal{O}(1\,\mu\mathrm{s})$. The state of the art algorithms used in this work [22,39] allow for a constant time step $\Delta t = 4\,\mu$s and relatively long physical simulation times up to $\mathcal{O}(10\,\mathrm{ms})$. In this case, the evolution of the turbulent sooting flame is integrated up to 20 ms in 5000 steps. Each simulation necessitates 18 million core hours on an IBM Blue Gene/P supercomputer, where the calculations are executed on 65 536 cores. Three such simulations at varying Da [23] are performed for a total of 54 million core hours and 100 TB of data produced.

In closing, we note that the present simulations resolve all length and time scales of momentum and gas-phase scalars fully. It is well known that resolution requirements for high Schmidt scalar transport are significantly more stringent than those for momentum and unity Schmidt scalars, thereby leading to prohibitive mesh sizes. In this work, the high Schmidt soot moments are solved by a Lagrangian particle method, which retains robustness and accuracy in the description of soot transport at the limited resolution afforded by a very large, albeit finite number of notional particles. As such, the numerical approach adopted here is best described as a DNS for the evolution of the momentum and gas-phase reactive scalars coupled with a robust and efficient Lagrangian model for soot transport. Finally, while the models for the chemistry of PAHs and for soot formation and growth are very detailed and state of the art, uncertainties in the description of these processes are well recognized and are the subject of ongoing research efforts.

3. Results

In this section, we will first point out selected flow features that are important for soot formation. The different time scales of combustion and pollutant formation are then discussed in comparison with the time scales of turbulent mixing. The discussion includes an assessment of the modelling implications for species governed by fast and slow time scales. The large Schmidt number of soot results in differential diffusion with respect to the gas phase. It will be shown that this is a leading order effect that depends on the fluctuations of scalar dissipation rate. Finally, it will be established that soot mass fraction is an intermittent field and it will be argued that this makes LES a particularly well-suited modelling approach for soot formation in turbulent flames.

(a) Overview of the flame

The overall features of the temporally evolving turbulent planar jet flame with the highest Damköhler number (Da_H) are shown in figure 1 at 15 ms. The fuel jet flows upwards along the periodic streamwise direction x and occupies the middle of the domain. The jet is surrounded by the air coflow moving downwards along the same axis. Figure 1*a* shows the field of mixture fraction Z, which quantifies the local fuel/air equivalence ratio normalized between zero (air) and one (fuel). Strong shear at the interface between the jet and the coflow results in the Kelvin–Helmholtz instability, which promotes the transition to turbulence and enhances mixing between the streams. The stoichiometric surface $Z_{st} = 0.147$ (blue colour isosurface in figure 1*a*) marks the location of a non-premixed flame between the jet core and the air coflow. It is apparent that turbulence bends and wrinkles the flame sheet, which displays a wide range of length scales. Turbulent mixing is characterized by large-scale structures (the 'rollers') as well as fine-scale flow features. The rollers are identified by areas of low mixture fraction gradients, two of which are apparent in the middle-left and top-right regions of the jet flame (figure 1*a*). The braid regions in between the rollers are marked by high strain. Regions of high strain are quite important for the dynamics of soot and its gas-phase precursors as will be discussed below.

In figure 1*b*, the spatial distribution of a selected isosurface of vorticity magnitude (grey colour) reveals that vorticity is highest on the fuel side and subsides near the flame sheet, identified by the temperature isosurfaces (light blue colour). In most turbulent non-premixed jet flames, the details of the flow in the fuel jet are of little consequence to the dynamics of the flame, which is located further away towards the oxidizer stream. For the present case, where soot formation is the focus of attention, the high values of vorticity in the rich region of the flame are significant, because they dictate the movement of soot particles as discussed later.

In figure 1*c*, naphthalene (yellow and red colour) is present on the rich side of the flame sheet (light blue colour) and abounds inside patches corresponding to the core of large-scale rollers in regions of low mixture fraction gradients (figure 1*a*). This feature has been noted in various experimental studies [19,20,43] and is explained by the persisting low values of scalar dissipation rate in the core of the rollers, compared with the high-strain braid regions [22]. Soot particles nucleate in regions of abundant naphthalene and continue to grow by condensation of aromatic molecules on their surface. The field of soot mass fraction is shown in figure 1*c* by isosurfaces corresponding to 10% of peak soot mass fraction (grey colour). The strong spatial variations observed for the soot precursors is exacerbated by the nonlinear dependence of soot growth on the local gas-phase composition, resulting in even greater scatter for the soot mass fraction field. At this time late into the evolution of the turbulent jet flame (15 ms), soot is present in large quantities everywhere in the fuel jet with the exception of the unmixed fuel stream, highlighting the role of turbulence in transporting soot across the domain. Soot is absent on the lean side of the flame because it is consumed by oxidation when it moves close to the flame sheet. When compared one to the other in figure 1*c*, the fields of temperature (light blue colour), naphthalene mass fraction (yellow and red colour) and soot mass fraction (grey colour) reveal a hierarchy of spatial–temporal inhomogeneity, with soot being organized in the smallest structures and temperature (or mixture fraction) in the largest.

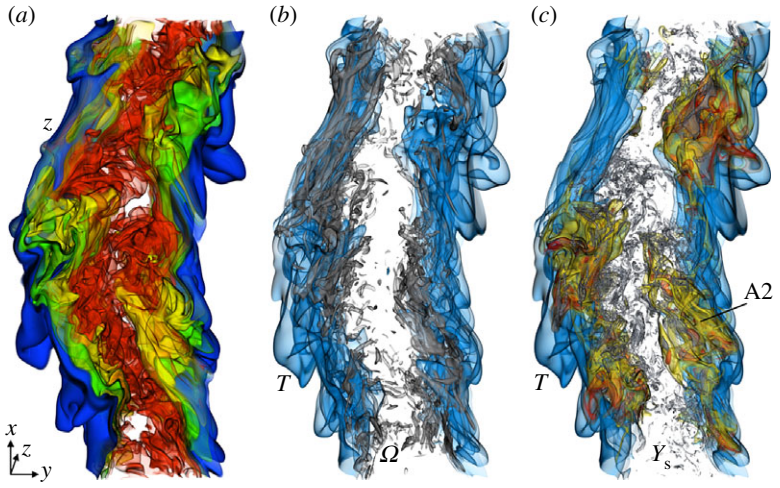

Figure 1. Renderings of instantaneous isosurfaces of various fields in the temporally evolving turbulent planar jet flame. The fuel jet flows from bottom to top along the *x*-axis and is surrounded by air moving downwards. (*a*) Mixture fraction $Z : Z_{st} = 0.147$ (blue), 0.3 (green), 0.5 (yellow) and 0.8 (red). (*b*) Vorticity magnitude $\Omega = 10^4\ s^{-1} \approx 20U_c/H$ (grey) and temperature $T = 1800$ K (light blue). (*c*) Naphthalene mass fraction $Y_{A2} = 200$ ppm (yellow) and 400 ppm (red), soot mass fraction $Y_s = 150$ ppm (grey) and $T = 1800$ K (light blue). Data from the turbulent jet flame with the highest Damköhler number (Da_H) at 15 ms [22].

(b) Statistics of soot precursors and soot formation

The mixture fraction is a conserved scalar, is independent of chemistry and is an important quantity in the theory and modelling of turbulent non-premixed flames [4]. Figure 2*a* shows the mean of temperature, naphthalene mass fraction and soot mass fraction conditioned on the local value of mixture fraction Z. The maximum value of the conditional mean of the temperature marks the flame sheet near $Z_{st} = 0.147$, where the stoichiometric ratio of fuel and oxidizer results in intense heat release rate and peak temperatures. The conditional mean of the naphthalene mass fraction peaks at a mixture fraction of 0.3 on the rich side of the flame sheet. The conditional mean of soot mass fraction peaks at $Z = 0.3$ also, due to rapid nucleation and intense soot growth rates at locations of abundant naphthalene.

The distribution of the conditional mean of naphthalene in mixture fraction space reflects the chemical pathways leading to the formation of benzene from intermediate species, here mostly the propargyl radical originating in the *n*-heptane decomposition layer on the rich side of the flame. It is important to note that in non-premixed flames, soot growth is mostly due to the condensation of PAHs on the surface of soot aggregates [18,21,22], rather than to surface reactions involving acetylene, i.e. the so-called HACA mechanism [37].

The conditional PDFs of temperature, naphthalene mass fraction and soot mass fraction are shown in figure 2*b* for $Z = 0.3$, which corresponds to the peak of the conditional means of naphthalene and soot mass fraction (figure 2*a*). These conditional PDFs are important in combustion modelling. In the limit of infinitely fast chemistry, all reactive scalars are functionally related to the mixture fraction. Then, the spatial distribution of temperature and species concentrations is uniquely determined by the distribution of Z and the conditional PDFs become delta functions. By contrast, the occurrence of broad conditional PDFs for reactive scalars is an indication of slow chemical reactions compared with mixing rates. In combustion research, the process by which turbulence and molecular mixing affect species concentrations and chemical reactions is referred to as 'turbulence–chemistry interaction' and has been the subject of vigorous research efforts for the past two decades, for instance, in the context of flame extinction [45] and NO_x formation [46].

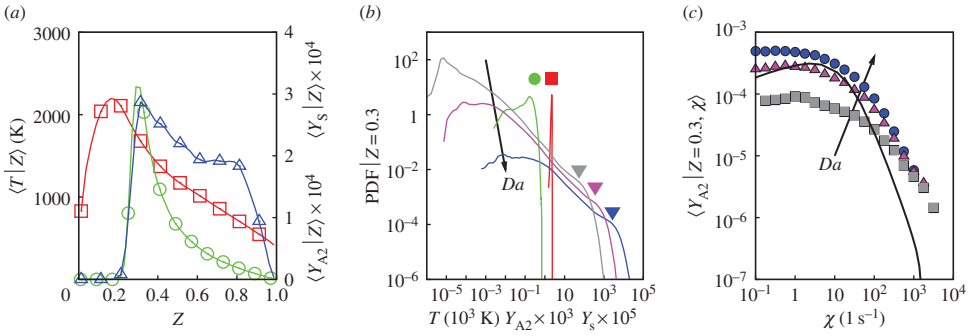

Figure 2. (*a*) Conditional mean of temperature T (red squares), naphthalene mass fraction Y_{A2} (green circles) and soot mass fraction Y_s (blue triangles). (*b*) Conditional PDF at $Z = 0.3$ of T (red line), Y_{A2} (green line) and Y_s (blue, purple and grey lines in order of decreasing *Da* number); conditional mean values are shown with solid symbols: T (red square), Y_{A2} (green circle) and Y_s (triangles). (*c*) Conditional mean of naphthalene mass fraction $\langle Y_{A2}|Z = 0.3, \chi\rangle$ at $Z = 0.3$ for various values of scalar dissipation rate χ: blue circles (Da_H), pink triangles (Da_M) and grey squares (Da_L) in order of decreasing *Da* number; the steady flamelet solution [4,44] with unity Lewis number for gas-phase species is also shown (black solid line). Data shown at 15 ms in the Da_H simulation [22,23], unless otherwise noted.

In the Da_H flow configuration, temperature is characterized by a very narrow distribution around its conditional mean $\langle T|Z\rangle$, implying that the chemistry of heat release is fast compared with mixing. On the other hand, the mass fraction of naphthalene displays a broad distribution around the mean (figure 2*b*), revealing turbulence–chemistry interaction with important implications for modelling of soot precursors.

The conditional PDFs of soot mass fraction for all three *Da* configurations are also shown in figure 2*b*. Although the ratio of the highest (Da_H) to the lowest Damköhler number (Da_L) is only four, the conditional mean of the soot mass fraction changes by two orders of magnitude among these cases, demonstrating the strongly nonlinear response of soot formation to variations in the rate of mixing. The soot PDFs are by far the broadest among those shown in figure 2*b*. This reflects the sensitivity of soot towards PAHs and that of the slow-forming PAH soot precursors to mixing. Further, soot transport effects contribute to broadening the distributions of soot mass fraction as will be explained later.

As the chemical reaction rates related to naphthalene are slow relative to mixing, a measure of the local mixing time scale is introduced in addition to mixture fraction to describe the species concentration. This local time scale of mixing is taken to be the inverse of the scalar dissipation rate $\chi = 2D|\nabla Z|^2$, where D is the thermal diffusion coefficient. Figure 2*c* shows the mean of the mass fraction of naphthalene conditioned on $Z = 0.3$ and various values of scalar dissipation rate χ. Results from simulations at all three Damköhler numbers [23] are reported together with those given by a one-dimensional, steady flamelet solution [4,44] with unity Lewis numbers for all gas-phase species. These results illustrate that the mass fraction of naphthalene drops sharply in response to increasing local scalar dissipation rate χ. This sensitivity of soot precursors to mixing rates was described experimentally in laminar counterflow experiments [47,48] and demonstrated by Bisetti *et al.* [21] in a DNS of soot formation in turbulent flames. We hasten to note that the sensitivity of the concentrations of soot precursors to the local gradients of mixture fraction implies a crucial dependence of soot formation and growth rates on the turbulent mixing process.

In addition, it is important to note the differences among the DNS results at a given χ and with respect to the flamelet solution (figure 2*c*). These differences establish that unsteady effects are important, as naphthalene does not adjust promptly to the instantaneous scalar dissipation rate due to its slow chemistry. These findings [21,22] motivated Mueller & Pitsch [26] to develop an LES closure based on a transport equation for naphthalene and adequate closure of its chemical source term. This circumvents the shortcomings of a steady flamelet approach and allows for the

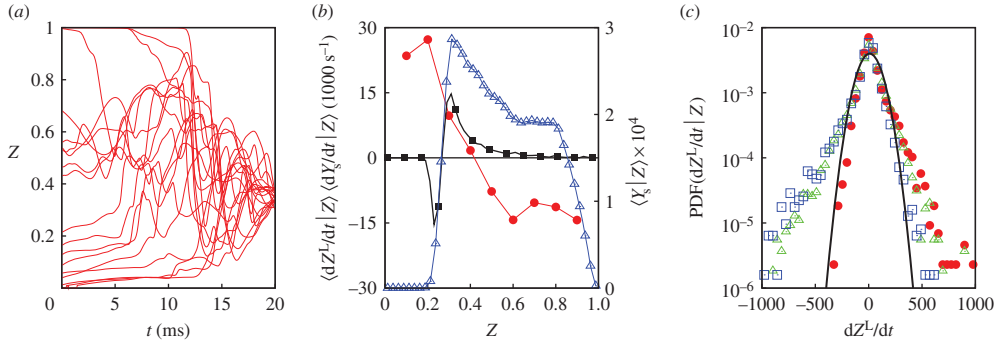

Figure 3. (*a*) Mixture fraction history along selected Lagrangian trajectories such that $Z \approx 0.3$ at 20 ms. (*b*) Conditional means of the Lagrangian derivative of mixture fraction $\mathrm{d}Z^{\mathrm{L}}/\mathrm{d}t$ (red solid circles), soot mass fraction Y_{s} (blue open triangles) and soot mass growth rate $\mathrm{d}Y_{\mathrm{s}}/\mathrm{d}t$ (black solid squares). (*c*) Conditional PDF of $\mathrm{d}Z^{\mathrm{L}}/\mathrm{d}t$ for $Z = 0.25$ (red solid circles), $Z = 0.5$ (green open triangles) and $Z = 0.75$ (blue open squares); for comparison, a Gaussian distribution fitted to the data for $Z = 0.5$ is shown (solid black line). Data from the Da_{H} simulation at 15 ms [22].

interaction of the time scales of turbulent mixing and those of the chemical reactions responsible for the formation of soot precursors, albeit at the resolved time and length scales of the filtered LES fields.

(c) Soot transport and differential diffusion effects

Soot transport is characterized by high Schmidt number or low diffusivity. Under standard atmospheric conditions, particles with a diameter of 10 nm (respectively, 100 nm) have a Schmidt number equal to 290 (respectively, 2.2×10^4) [49, p. 34]. As a consequence, diffusive transport of soot is negligible and soot aggregates move along flow pathlines, experiencing differential diffusion effects akin to those that occur among gas-phase species of disparate molecular weights. Differential diffusion between soot and gas-phase species manifests itself as a movement of soot in mixture fraction space. This drift of soot in Z-space (as well as in temperature and composition spaces) has important consequences for the growth rates of soot, which depend on the local mixture's temperature and concentration of soot precursors. The statistics of soot drift are connected intimately to those of turbulent mixing and are conveniently described in a Lagrangian frame. In passing, we note that issues related to drift in mixture fraction space are not unique to soot, rather are characteristic of all aerosol flows in spatially inhomogeneous mixing fields [50].

Figure 3*a* portrays the evolution of mixture fraction $Z^{\mathrm{L}}(t)$ along a handful of Lagrangian trajectories. Selected particle trajectories, for which the mixture fraction is $Z \approx 0.3$ at 20 ms, are shown. It is apparent that the fluid parcels originate from disparate locations in the layer at time zero and undergo dissimilar trajectories in mixture fraction space, so that different soot aggregates experience disparate histories of gas-phase temperature and composition. The sudden jumps in mixture fraction along the trajectories reflect the intermittent nature of the scalar dissipation rate field. These jumps may be quite important for the soot evolution owing to the strongly nonlinear dependence of soot growth and oxidation rates on the mixture composition as explained below.

The time derivative of $Z^{\mathrm{L}}(t)$ is referred to as the 'Lagrangian derivative of mixture fraction' and given the symbol $\mathrm{d}Z^{\mathrm{L}}/\mathrm{d}t$. Note that $\mathrm{d}Z^{\mathrm{L}}/\mathrm{d}t = \nabla \cdot (\rho D \nabla Z)/\rho$ according to the conservation equation for mixture fraction. The Lagrangian derivative of Z quantifies the rate of soot drift in mixture fraction space due to differential diffusion as soot travels within a fluid parcel across the domain. Figure 3*b* shows the conditional mean $\langle \mathrm{d}Z^{\mathrm{L}}/\mathrm{d}t|Z \rangle$, which describes the global mixing process in the jet: on average, fluid parcels with $Z \leq 0.4$ move towards richer mixture fraction values, while the opposite is true for $Z > 0.4$.

Figure 3*b* shows again the conditional mean of soot mass fraction $\langle Y_s|Z\rangle$ and also the rate of change of soot mass fraction $\langle dY_s/dt|Z\rangle$. Soot mass fraction is distributed broadly in mixture fraction space in the range $0.2 \leq Z < 1$, i.e. on the rich side of the flame located at $Z_{st} = 0.147$. However, in regions with $Z \geq 0.6$, the net soot growth rate is essentially zero and the mean drift is towards leaner values. This is also the case for earlier times prior to 15 ms. This leaves the question of why soot appears in large amounts in the very rich part of the flame.

A clue to resolving this question lies in the statistics of the fluctuations of dZ^L/dt brought by turbulent mixing. Figure 3*c* shows the PDF of dZ^L/dt for various conditioning values of Z. The PDFs display wide tails and drift events with rates much larger than the mean rate of drift occur with non-negligible frequency. For example, the PDF for $Z = 0.5$ documents events of rapid soot drift towards richer mixtures and against the negative mean drift. These events allow for the presence of soot at very large values of mixture fraction deep into the fuel layer. Thus, the intermittent mixing field plays a key role in spreading soot in mixture fraction space, and its effect is not represented adequately by the mean mixing process in the jet [22].

Soot transport in mixture fraction space is not solely responsible for the distribution of soot, and $\langle Y_s|Z\rangle$ is governed by the combination of drift and growth processes, which depend on the gas-phase composition and temperature [22]. For instance, upon nucleating at $Z = 0.3$, soot moving towards leaner mixtures is rapidly and entirely consumed by oxidation. This is shown in figure 3*b*, where a negative overall rate of change of Y_s occurs for $Z \leq 0.25$. On the contrary, soot moving towards richer mixtures grows slowly in the range $0.3 \leq Z \leq 0.6$ and avoids oxidation near the flame. The combined action of drift and soot growth away from the flame sheet and destruction near the reaction zone results in soot being distributed preferentially at rich mixture fraction values [22]. We conclude that the effects of fluctuating differential diffusion are of leading order and need to be considered in combustion models. However, adequate modelling strategies have not been developed so far.

(d) Large-scale soot intermittency

The spatial distribution of soot mass fraction is depicted in figure 4*a*, where isocontours of Y_s are portrayed on an $x - y$ plane. Consistently with the qualitative appearance of the three-dimensional soot field in figure 1*c*, soot mass fraction displays a wide range of length scales. Soot occupies regions as large as the largest flow structures in the jet (rollers) as shown by a large patch of soot located on the right side towards the middle of the domain in figure 4*a*. Peaks in soot mass fraction are organized in small and elongated structures located within larger regions characterized by non-negligible, albeit lower values of soot mass fraction.

Figure 4*b–d* shows the naphthalene mass fraction, soot number density and soot mass fraction fields in a small area of the domain occupied by large-scale flow structures (see yellow box in the bottom-right corner of figure 4*a*). A qualitative, visual comparison between the Y_{A2} and N_s fields (figure 4*b*,*c*) reveals that the peak values of number density and naphthalene mass fraction occur at the same locations. This behaviour is due to intense nucleation of new particles at locations of abundant naphthalene and the ensuing coagulation, which decreases the particle number in regions where the concentration of naphthalene is low. As a result, the smallest spatial features of N_s resemble those of the Y_{A2} field [22].

A strong spatial correlation is not apparent between peaks of Y_{A2} and peaks of Y_s (figure 4*b*,*d*. There are regions of the flow where the naphthalene mass fraction is highest, but soot mass fraction is negligible and vice versa. For example, this occurs at selected locations in the bottom-right corner of figure 4*b*,*d*). Owing to its slow growth rates, there may be little soot mass at locations of abundant naphthalene. Furthermore, regions where soot mass fraction is high, yet naphthalene is absent, are explained by soot mass fraction remaining constant as soot drifts into regions characterized by negligible naphthalene.

The isocontours at 0.1 and 1% of the peak values for the three fields of interest are shown in figure 4*b–d*. The two contours are almost identical for all three fields Y_{A2}, N_s and Y_s and overlap for the most part. Thus, these isocontours may be taken to identify a sharp interface

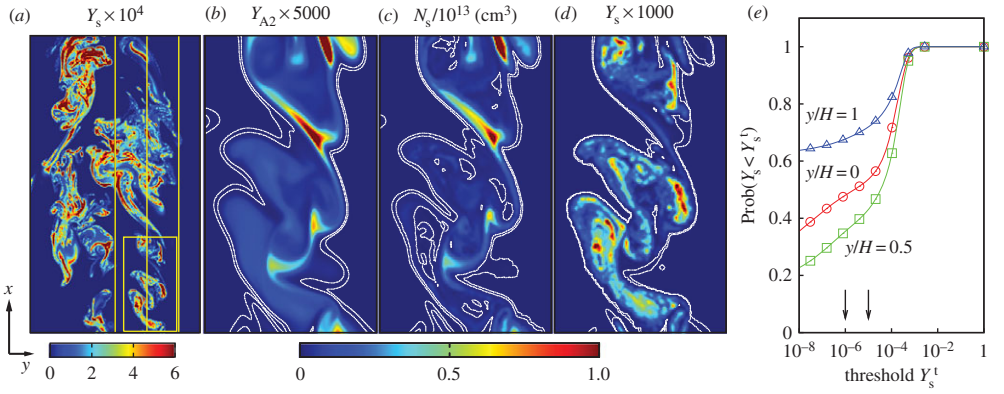

Figure 4. (*a*) Contour plot of soot mass fraction on an x–y plane covering the entire streamwise extent of the domain; the yellow vertical lines mark three crosswise locations (left to right): $y/H = 0$, 0.5 and 1. (*b–d*) Contour plots of the naphthalene mass fraction Y_{A2}, soot number density N_s and soot mass fraction Y_s in the region of the domain delimited by the yellow rectangle in (*a*); isocontours at 0.1 and 1% of peak value for each field are shown as white solid lines. (*e*) Intermittency parameter reflecting Prob($Y_s < Y_s^t$) at the crosswise locations marked by the yellow vertical lines in (*a*) as a function of the threshold Y_s^t; 0.1 and 1% of peak value of soot mass fraction indicated by vertical arrows. Data from the Da_H simulation at 15 ms.

separating regions of the flow where naphthalene and soot are present from those where they are negligible. It is evident that the isocontours envelop large flow structures characteristic of shear flow. In the case of number density N_S (figure 4*c*), there exist small regions inside the large structures with values below the threshold. Further, these small regions correspond to locations where the soot mass fraction is highest (figure 4*d*). This occurrence is due to coagulation lowering the soot number density, as soot growth leads to an increase in soot mass fraction and suppresses nucleation of new particles by scavenging gas-phase precursors.

Recently, the concept of 'soot intermittency' and a related intermittency parameter have been introduced in various experimental and numerical studies of soot formation in turbulent flames [19,26,27]. The soot intermittency parameter at a spatial location is defined as the probability that the soot volume fraction is less than a small threshold at any given time. Qamar *et al.* [19] measured soot volume fraction in a turbulent non-premixed round jet flame of natural gas and air (known as the 'Delft Flame III' [51]). They defined the threshold to be 0.1 ppb (≈0.1% of instantaneous peak values of soot volume fraction) and reported an intermittency above 0.96 for all locations along the jet centreline and up to 140 diameters downstream of the nozzle.

The intermittency parameter is computed based on the high Da number DNS data (Da_H) and shown in figure 4*e*. The parameter is computed at three crosswise locations in the flame and for a wide range of threshold values. While the values of the intermittency parameter shown in figure 4*e* are different from those found by Qamar *et al.* [19], soot intermittency is observed for the turbulent flame considered here also, in agreement with experiments [19]. As it will be argued below, discrepancies in the values of intermittency are most likely due to the flow configurations being different. For a given value of the threshold, the intermittency parameter differs among the three crosswise locations considered, being highest for $y/H = 1$ (highest probability of soot mass fraction below the threshold) and lowest for $y/H = 0.5$. By and large, the differences in intermittency reflect the crosswise distribution of the mean soot mass fraction, which is highest at $y/H = 0.5$, slightly lower on the jet axis ($y/H = 0$), and lowest on the outer edge of the soot layer towards the flame sheet ($y/H = 1$) [22]. At all crosswise locations, the intermittency parameter decreases rapidly as the threshold decreases from $Y_s^t = 10^{-3}$ to 10^{-5}, the latter value corresponding to ≈1% of peak mass fraction. Below $Y_s^t = 10^{-5}$, the sensitivity of the parameter to the threshold is significantly lower, justifying the usage of threshold values $Y_s^t \leq 10^{-5}$ to measure soot intermittency. The values $Y_s^t = 10^{-6}$ and 10^{-5} are marked in figure 4*e* and correspond to the

isocontours at 0.1 and 1% of peak mass fraction shown in figure 4*b–d*. These isocontours were shown to envelop the large scales of the flow and provide a good measure of soot intermittency. The appearance of the soot fields in figure 4*a–d* and the analysis of the intermittency parameter based on the DNS data suggest that soot intermittency is connected with soot patches coinciding with large flow structures ('large-scale soot intermittency'). In the core of these structures, where low values of scalar dissipation rate persist for relatively long periods of time, soot precursors abound and foster soot growth.

Owing to the dependence of soot on large-scale flow features, the intermittency parameter and the spatial distribution of soot are likely to be specific to the flow configuration as well as the stage of the development of turbulence. The results shown in two- and three-dimensional simulations [21–24,26,28,52] and experimental studies [19,20] of turbulent sooting flames support this observation. Qamar *et al.* [19] investigated soot formation in a turbulent round jet flame of methane and air and provided instantaneous snapshots of the soot volume fraction field via laser-induced incandescence. Given the low sooting propensity of methane, soot forms far downstream of the inlet, where soot appears in the form of patches of size comparable to the jet width. It is apparent that, based on their size, these soot patches are connected with the largest structures of the flow in the far field of the jet. This feature is well captured by a recent LES study [26] of the same turbulent jet flame.

Large-scale soot intermittency and its strong relation with the unsteady dynamics of mixing and soot precursors has important implications for subfilter-scale closure models in LES of turbulent sooting flames. LES resolves the unsteady motion of large-scale flow structures of turbulent fields and is able to simulate flow features, which are specific to the configuration of interest. Thus, the large-scale regions of abundant soot and related intermittency are likely to be captured by the resolved (filtered) soot fields, provided that models addressing unsteady effects in the evolution of the soot precursors are employed. Fortunately, recently proposed unsteady subfilter closures for LES [5] may be readily adapted to the description of soot precursor species. On the other hand, closures for Reynolds-averaged approaches must model the effect of intermittency on soot dynamics entirely. Owing to the strongly nonlinear source terms governing soot formation and growth and the flow-specificity of intermittency, this appears to be an extremely difficult, if not impossible undertaking. Despite its potential for soot predictions, LES will most likely require modelling of the subfilter contributions of the filtered source terms for selected soot processes. For example, one may expect that coagulation rates need a subfilter closure due to the unresolved, small-scale features of soot number density and the strong nonlinearities in the functional expressions. Nonetheless, compared to RANS methods, which do not resolve the unsteady motion of large scales, LES provides a much more advantageous framework for the development of predictive models for soot formation in turbulent combustion.

4. Conclusion

The development of efficient and ultra-low emission combustion devices is a pivotal component of a realistic strategy for the abatement of the emissions of anthropogenic carbon. Notwithstanding the current usage of CFD in the design cycle of combustors and engines, combustion models are far from being predictive, especially with regard to pollutant emissions. Modelling pollutant formation in turbulent combustion is challenging owing to the strongly nonlinear behaviour of the chemical source terms and to the vast range of time and length scales of flow and chemistry.

Data from DNS studies are often helpful for modelling purposes in non-reactive fluid mechanics. This statement is even more applicable to combustion problems, where detailed joint data of reactive scalars and flow field are scarce, so that DNS provides unique and invaluable information for understanding nonlinear processes and interactions, thereby accelerating and enabling model development and validation. Here, the use of DNS for combustion modelling has been demonstrated by addressing a particularly challenging topic in turbulent combustion, the formation, transport and oxidation of soot.

Based on DNS studies of time-evolving, periodic, turbulent non-premixed *n*-heptane/air planar jet flames for constant *Re* and varying *Da* number, the features of soot formation and growth in turbulent flames were analysed and the implications for modelling discussed. It was found that, compared with the heat release chemistry, the time scales of the formation of PAH and soot are always slow and the effective Damköhler numbers for these processes therefore small under realistic flow conditions. Further, transport of soot particles leads to differential diffusion with respect to the gas phase. The resulting effect is important and was shown to depend on the fluctuations of scalar dissipation rate, which are not considered in present-day LES subfilter models. Finally, the intermittency of the soot mass fraction in the turbulent field was discussed, shown to occur on the large scales and argued to be flow specific, so that it should be well captured by LES.

DNS for turbulent combustion was shown to provide invaluable data. Data for moderate Reynolds number flows and detailed descriptions of physico-chemical processes enable model advancement, which would be impossible otherwise. It is expected that eddy-resolving simulations will play a central role in the design of future engines and combustors and that DNS databases will become increasingly important for subfilter model development, thereby supporting the broad goals of carbon abatement and pollutant reduction.

Acknowledgements. The three-dimensional renderings of the turbulent flame in figure 1 were produced by Dr Madhusudhanan Srinivasan at the KAUST Visualization Laboratory (KVL).

Funding statement. Research reported in this publication was supported by the King Abdullah University of Science and Technology (KAUST) through the Competitive Research Grant 1 (CRG-1) program. The authors acknowledge valuable support from KAUST Supercomputing Laboratory (KSL) in the form of computational time on the IBM Blue Gene/P System 'Shaheen'.

References

1. International Energy Agency. 2013 *World energy outlook 2013*. Paris, France: IEA Publications. See http://www.worldenergyoutlook.org.
2. Bilger RW, Pope SB, Bray KNC, Driscoll JF. 2005 Paradigms in turbulent combustion research. *Proc. Combust. Inst.* **30**, 21–42. (doi:10.1016/j.proci.2004.08.273)
3. Frisch U. 1996 *Turbulence: the legacy of A. N. Kolmogorov*. Cambridge, UK: Cambridge University Press.
4. Peters N. 2000 *Turbulent combustion*. Cambridge, UK: Cambridge university press.
5. Pitsch H. 2006 Large-eddy simulation of turbulent combustion. *Annu. Rev. Fluid Mech.* **38**, 453–482. (doi:10.1146/annurev.fluid.38.050304.092133)
6. Gicquel LY, Staffelbach G, Poinsot T. 2012 Large eddy simulations of gaseous flames in gas turbine combustion chambers. *Prog. Energy Combust. Sci.* **38**, 782–817. (doi:10.1016/j.pecs.2012.04.004)
7. Chen JH. 2011 Petascale direct numerical simulation of turbulent combustion: fundamental insights towards predictive models. *Proc. Combust. Inst.* **33**, 99–123. (doi:10.1016/j.proci.2010.09.012)
8. Ihme M, Cha CM, Pitsch H. 2005 Prediction of local extinction and re-ignition effects in non-premixed turbulent combustion using a flamelet/progress variable approach. *Proc. Combust. Inst.* **30**, 793–800. (doi:10.1016/j.proci.2004.08.260)
9. Yang Y, Wang H, Pope SB, Chen JH. 2013 Large-eddy simulation/probability density function modeling of a non-premixed co/H_2 temporally evolving jet flame. *Proc. Combust. Inst.* **34**, 1241–1249. (doi:10.1016/j.proci.2012.08.015)
10. Knudsen E, Richardson E, Doran E, Pitsch H, Chen J. 2012 Modeling scalar dissipation and scalar variance in large eddy simulation: algebraic and transport equation closures. *Phys. Fluids* **24**, 055103. (doi:10.1063/1.4711369)
11. Charlette F, Meneveau C, Veynante D. 2002 A power-law flame wrinkling model for LES of premixed turbulent combustion Part II: dynamic formulation. *Combust. Flame* **131**, 181–197. (doi:10.1016/S0010-2180(02)00401-7)
12. Moureau V, Domingo P, Vervisch L. 2011 From large-eddy simulation to direct numerical simulation of a lean premixed swirl flame: filtered laminar flame-pdf modeling. *Combust. Flame* **158**, 1340–1357. (doi:10.1016/j.combustflame.2010.12.004)

13. Hawkes ER, Chatakonda O, Kolla H, Kerstein AR, Chen JH. 2012 A petascale direct numerical simulation study of the modelling of flame wrinkling for large-eddy simulations in intense turbulence. *Combust. Flame* **159**, 2690–2703. (doi:10.1016/j.combustflame.2011.11.020)
14. Karpetis AN, Barlow RS. 2005 Measurements of flame orientation and scalar dissipation in turbulent partially premixed methane flames. *Proc. Combust. Inst.* **30**, 665–672. (doi:10.1016/j.proci.2004.08.222)
15. Donaldson K, Tran L, Jimenez LA, Duffin R, Newby DE, Mills N, MacNee W, Stone V. 2005 Combustion-derived nanoparticles: a review of their toxicology following inhalation exposure. *Part. Fibre Toxicol.* **2**, 1–14. (doi:10.1186/1743-8977-2-10)
16. Jacobson MZ. 2001 Strong radiative heating due to the mixing state of black carbon in atmospheric aerosols. *Nature* **409**, 695–697. (doi:10.1038/35055518)
17. Bockhorn H. 1994 *Soot formation in combustion*. New York, NY: Springer.
18. Wang H. 2011 Formation of nascent soot and other condensed-phase materials in flames. *Proc. Combust. Inst.* **33**, 41–67. (doi:10.1016/j.proci.2010.09.009)
19. Qamar NH, Alwahabi ZT, Chan QN, Nathan GJ, Roekaerts D, King KD. 2009 Soot volume fraction in a piloted turbulent jet non-premixed flame of natural gas. *Combust. Flame* **156**, 1339–1347. (doi:10.1016/j.combustflame.2009.02.011)
20. Bockhorn H, Geitlinger H, Jungfleisch B, Lehre T, Schön A, Streibel T, Suntz R. 2002 Progress in characterization of soot formation by optical methods. *Phys. Chem. Chem. Phys.* **4**, 3780–3793. (doi:10.1039/b201071b)
21. Bisetti F, Blanquart G, Mueller ME, Pitsch H. 2012 On the formation and early evolution of soot in turbulent nonpremixed flames. *Combust. Flame* **159**, 317–335. (doi:10.1016/j.combustflame.2011.05.021)
22. Attili A, Bisetti F, Mueller ME, Pitsch H. 2014 Formation, growth, and transport of soot in a three-dimensional turbulent non-premixed jet flame. *Combust. Flame.* **161**, 1849–1865. (doi:10.1016/j.combustflame.2014.01.008)
23. Attili A, Bisetti F, Mueller ME, Pitsch H. In press. Damköhler number effects on soot formation and growth in turbulent nonpremixed flames. *Proc. Combust. Inst.* **35**.
24. Lignell DO, Chen JH, Smith PJ. 2008 Three-dimensional direct numerical simulation of soot formation and transport in a temporally evolving nonpremixed ethylene jet flame. *Combust. Flame* **155**, 316–333. (doi:10.1016/j.combustflame.2008.05.020)
25. El-Asrag H, Menon S. 2009 Large eddy simulation of soot formation in a turbulent non-premixed jet flame. *Combust. Flame* **156**, 385–395. (doi:10.1016/j.combustflame.2008.09.003)
26. Mueller ME, Pitsch H. 2012 LES model for sooting turbulent nonpremixed flames. *Combust. Flame* **159**, 2166–2180. (doi:10.1016/j.combustflame.2012.02.001)
27. Mueller ME, Chan QN, Qamar NH, Dally BB, Pitsch H, Alwahabi ZT, Nathan GJ. 2013 Experimental and computational study of soot evolution in a turbulent nonpremixed bluff body ethylene flame. *Combust. Flame* **160**, 1298–1309. (doi:10.1016/j.combustflame.2013.02.010)
28. Yoo CS, Im HG. 2007 Transient soot dynamics in turbulent nonpremixed ethylene-air counterflow flames. *Proc. Combust. Inst.* **31**, 701–708. (doi:10.1016/j.proci.2006.08.090)
29. Blanquart G, Pitsch H. 2009 A joint volume-surface-hydrogen multi-variate model for soot formation. In *Combustion generated fine carbonaceous particles* (eds H Bockhorn, A D'Anna, AF Sarofim, H Wang), pp. 437–463. Karlsruhe, Germany: KIT Scientific Publishing.
30. Mueller ME, Pitsch H. 2011 Large eddy simulation subfilter modeling of soot–turbulence interactions. *Phys. Fluids* **23**, 115 104–115 104. (doi:10.1063/1.3657826)
31. Müller B. 1999 Low Mach number asymptotics of the Navier–Stokes equations and numerical implications. In *30th Computational Fluid Dynamics* (ed. H Deconinck). Lecture Series, vol. 1999-03. Brussels, Belgium: von Karman Institute for Fluid Dynamics.
32. Poinsot T, Veynante D. 2005 *Theoretical and numerical combustion*. Philadelphia, PA: RT Edwards, Inc.
33. Mueller ME, Blanquart G, Pitsch H. 2009 A joint volume-surface model of soot aggregation with the method of moments. *Proc. Combust. Inst.* **32**, 785–792. (doi:10.1016/j.proci.2008.06.207)
34. Frenklach M. 2002 Method of moments with interpolative closure. *Chem. Eng. Sci.* **57**, 2229–2239. (doi:10.1016/S0009-2509(02)00113-6)

35. Mueller ME, Blanquart G, Pitsch H. 2009 Hybrid method of moments for modeling soot formation and growth. *Combust. Flame* **156**, 1143–1155. (doi:10.1016/j.combustflame 2009.01.025)
36. Blanquart G, Pitsch H. 2009 Analyzing the effects of temperature on soot formation with a joint volume-surface-hydrogen model. *Combust. Flame* **156**, 1614–1626. (doi:10.1016/j. combustflame.2009.04.010)
37. Frenklach M, Wang H. 1991 Detailed modeling of soot particle nucleation and growth. *Proc. Combust. Inst.* **23**, 1559–1566. (doi:10.1016/S0082-0784(06)80426-1)
38. Kazakov A, Wang H, Frenklach M. 1995 Detailed modeling of soot formation in laminar premixed ethylene flames at a pressure of 10 bar. *Combust. Flame* **100**, 111–120. (doi:10.1016/0010-2180(94)00086-8)
39. Desjardins O, Blanquart G, Balarac G, Pitsch H. 2008 High order conservative finite difference scheme for variable density low Mach number turbulent flows. *J. Comput. Phys.* **227**, 7125–7159. (doi:10.1016/j.jcp.2008.03.027)
40. Attili A, Bisetti F. 2013 Application of a robust and efficient Lagrangian particle scheme to soot transport in turbulent flames. *Comput. Fluids* **84**, 164–175. (doi:10.1016/j. compfluid.2013.05.018)
41. Wright D. 2007 Numerical advection of moments of the particle size distribution in Eulerian models. *J. Aerosol Sci.* **38**, 352–369. (doi:10.1016/j.jaerosci.2006.11.011)
42. LeVeque R, Yee H. 1990 A study of numerical methods for hyperbolic conservation laws with stiff source terms. *J. Comput. Phys.* **86**, 187–210. (doi:10.1016/0021-9991(90)90097-K)
43. Pickett LM, Ghandhi JB. 2003 Structure of a reacting hydrocarbon-air planar mixing layer. *Combust. Flame* **132**, 138–156. (doi:10.1016/S0010-2180(02)00431-5)
44. Pitsch H. 1998 FlameMaster, a C++ computer program for 0D combustion and 1D laminar flame calculations. Technical report, University of Technology (RWTH), Aachen, Germany.
45. Barlow R, Frank J. 1998 Effects of turbulence on species mass fractions in methane/air jet flames. *Proc. Combust. Inst.* **27**, 1087–1095. (dopi:10.1016/S0082-0784(98)80510-9)
46. Driscoll JF, Chen RH, Yoon Y. 1992 Nitric oxide levels of turbulent jet diffusion flames: effects of residence time and damkohler number. *Combust. Flame* **88**, 37–49. (doi:10.1016/ 0010-2180(92)90005-A)
47. Tsuji H, Yamaoka I. 1969 The structure of counterflow diffusion flames in the forward stagnation region of a porous cylinder. *Proc. Combust. Inst.* **12**, 997–1005. (doi:10.1016/ S0082-0784(69)80478-9)
48. Du DX, Axelbaum RL, Law CK. 1989 Experiments on the sooting limits of aerodynamically-strained diffusion flames. *Proc. Combust. Inst.* **22**, 387–394. (doi:10.1016/ S0082-0784(89)80045-1)
49. Friedlander SK. 2000 *Smoke, dust and haze: fundamentals of aerosol behavior*. New York, NY: Oxford University Press.
50. Zhou K, Attili A, Alshaarawi A, Bisetti F. In press. Simulation of aerosol nucleation and growth in a turbulent mixing layer. *Phys. Fluids.*
51. Peeters TWJ, Stroomer PPJ, de Vries JE, Roekaerts DJEM. 1994 Comparative experimental and numerical investigation of a piloted turbulent natural-gas diffusion flame. *Proc. Combust. Inst.* **25**, 1241–1248. (doi:10.1016/S0082-0784(06)80764-2)
52. Lignell DO, Chen JH, Smith PJ, Lu T, Law CK. 2007 The effect of flame structure on soot formation and transport in turbulent nonpremixed flames using direct numerical simulation. *Combust. Flame* **151**, 2–28. (doi:10.1016/j.combustflame.2007.05.013)